Improvement of an Oak Canopy Model Extracted from Digital Photogrammetry

Peng Gong, Xueliang Mei, Gregory S. Biging, and Zuxun Zhang

Abstract

Digital surface models (DSMs) automatically derived with digital photogrammetric systems are useful in land surface change monitoring, including forest growth monitoring. However, they cannot be applied directly to forest canopy change analysis with high accuracy due to the inevitable deficiencies in existing commercial digital photogrammetry packages. In a hardwood rangeland monitoring study, we found that the oak tree and woodland canopy boundaries were not well determined using several digital photogrammetry packages available to us. There was a noticeable discrepancy between the true crown closure and that determined by subtracting the DSM and the corresponding DEM that excludes tree heights. In this paper, we present a correction method for improvement at the erroneous canopy boundary locations in the DSM using shadow and boundary information extracted from imagery. The method is designed for correcting errors for broadleaf tree canopies. Aerial photographs taken over oak woodland hills were tested. Using manual photogrammetric measurements as the reference, we found that most of the points (88.3 percent) on the canopy boundaries were displaced by greater than 1 meter with a conventional digital photogrammetric package. After the proposed algorithms were applied, greater than 98.6 percent of the points on canopy boundaries were found to be within 1 meter of their reference positions. 78.4 percent of the reference points had greater than 2 meters elevation errors with the conventional package while greater than 85.6 percent of those points were found to be within 2 meters of the reference after the proposed algorithms were applied.

Introduction

Digital surface models (DSMs) automatically derived using digital photogrammetry systems have been applied to topographic mapping (e.g., Ackerman and Krzystek, 1997), image understanding (Weidner and Förstner, 1995), and change monitoring (Gong *et al.*, 1999a; Gong *et al.*, 1999b; Brown and Arbogast, 1999). Since 1995, we have been developing DSM-based techniques for monitoring changes in California's oak woodlands (Gong *et al.*, 1999b). DSMs from two different dates extracted over the same area were first automatically derived from aerial photographs using digital photogrammetry systems. Individual tree growth, loss of trees from mortality or cutting, and regenerated trees were then detected by subtracting one DSM from the other. Although the approach was promising in forest change monitoring, we found that DSMs thus derived were not reliable and were often erroneous at locations where elevation changes abruptly, e.g., at borders of forest or individual tree canopy. Thus, it is difficult to obtain reliable results for forest monitoring before some post-processing is applied to the multidate DSMs.

Based on our analysis, we found that errors in DSMs derived from digital photogrammetry were primarily from image matching. In image matching, surface smoothness is used as a constraint in most of the commercial packages. The purpose of the smoothness constraint is to reduce abrupt changes and eliminate non-topographic scene components in order to derive accurate surface elevation. This constraint may not be applicable in image areas where non-topographic components are desirable. Standing objects such as buildings, oak trees, and other forest stands cannot be treated as a cohesive unit on a stereo pair of aerial photographs. The depth (elevation) discontinuities at the boundaries of forest stands divide the whole underlying surface into many piecewise patches. Within each individual patch the surface can be approximately treated as continuously smooth, i.e., the individual surface patch satisfies the so-called smoothness constraint. Therefore, the underlying surface should first be separated in advance. Then the smoothness constraint can be applied properly to each individual surface patch. Furthermore, depth discontinuities may lead to occlusions, which are portions of the ground not seen on one of the two images. Occlusions lead to "null" matches. The occluded regions caused by perspective projection during aerial photography should be excluded from the matching process. Unfortunately, this is not done in most existing image matching algorithms because they are designed for topographic mapping where occlusions usually do not occur. Thus, in the final 3D surface data, the occluded regions may be derived from false matches or "blind" interpolation. In our study, the "blind" interpolation is usually fitting between the ground surface and tree canopy. This leads to an expansion of forest stands at forest boundaries. Boundaries of standing objects at occluded areas are shifted because of smoothing. Therefore, 3D data obtained over occluded areas are erroneous.

Because of the two shortcomings described above, the final DSM becomes continuously smooth, and important features such as depth discontinuities caused by standing objects are not captured. We need to use boundary information to prevent the smoothness constraint from being employed at the boundaries of standing objects such as forest stands and to assist in the detection of occluded regions. To achieve this goal, a boundary constraint and an occlusion constraint should be applied in image

P. Gong is with the International Institute for Earth System Science, Nanjing University, Nanjing, China 210093 and the Center for Assessment and Monitoring of Forest and Environmental Resources (CAMFER), 151 Hilgard Hall, University of California, Berkeley, CA 94720-3110 (gong@nature.berkeley.edu).

X. Mei and G.S. Biging are with CAMFER, University of California, Berkeley, CA 94720-3110.

Z. Zhang is with the Department of Photogrammetry, Wuhan University, Wuhan, P. R. China.

Photogrammetric Engineering & Remote Sensing
Vol. 63, No. 9, September 2002, pp. 919–924.

0099-1112/02/6809–919$3.00/0

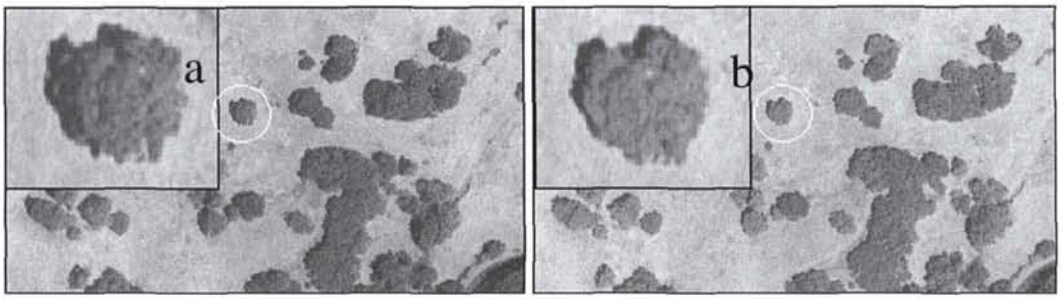

Figure 1. A portion of a stereopair of aerial photographs acquired over an oak woodland stand in Lucas Valley, Marin County, California.

matching. In addition, shadows exist when aerial photography is taken under sunny conditions. The shadow geometry can also be used as a constraint because shadows of tree canopy represent areas substantially lower in elevation than the canopy surface.

Given the above considerations, one option is to develop a new image matching algorithm that takes those new constraints into consideration. This takes a considerable amount of time and resources to accomplish. Mohan *et al.* (1989) demonstrate that substantial improvements in the overall performance of the entire digital photogrammetric procedure can be achieved by applying some of the constraint information after image matching is done. We decided to take advantage of the existing algorithms (Dhond and Aggrawal, 1989; Heipke, 1996; Mei *et al.*, 2001) and apply the new constraints through postprocessing.

The objective of this study was to improve the accuracy of a DSM of an oak woodland stand using a stereo-pair of aerial photographs. Because the inner portion of an oak tree crown surface is relatively smooth, it can be derived with relatively high accuracy by using existing commercial software packages. The challenge was to accurately recover the crown margins near the outer portions of tree crowns because abrupt elevation changes at the crown margins lead to large uncertainties in image matching.

Obtaining the DSM

The DSM can be automatically derived using digital photogrammetric systems such as Socket Set, Match-T, and VirtuoZo™. This can be done using a standard digital photogrammetric procedure. The procedure normally consists of six steps. They are interior orientation, relative orientation and generation of epipolar images, absolute orientation, image matching, and interpolation and generation of DSM. Among them, the matching process is vital to the whole procedure. Although there are two major categories of image matching algorithms in the literature—area-based and feature-based—most built-in algorithms in commercial digital photogrammetric systems are area-based. For example, VirtuoZo™, the one we used for our study, employs an area-based image matching algorithm (http://www.virtuozo.com.au).

An aerial stereo-pair acquired over an oak woodland area was scanned at a 25-μm resolution (Figure 1). It was acquired over Lucas Valley (38°02′38″W, 122°36′30″N), Marin County, California, with a nominal scale of 1:12,000. An individual oak tree on a 23.4° hill slope with a height of approximately 10.3 meters was enlarged (Figure 1). The black-and-white photographs were taken around 2:30 PM local time (it was estimated from the sun angle and the geographic location due to the lack of the time information) in August, 1995. The solar elevation and azimuth were 55°02′38″ and 64°02′38″, respectively (determined from measurements of several points and their shadow points). From Figure 1, we can see that three classes may be found: background dry grasses, shadows, and forest stands (field visitation indicated that the stands were primarily oak trees). Shadows are the darkest and the background is white, while the forest stands appear grey. Our experiments indicated that methods such as gray-level thresholding worked well in separating them.

Ground control points (GCPs) were collected using geodetic quality GPS receivers operated in the differential mode. Absolute orientation was done using GCPs. Following a standard photogrammetric procedure, the initial DSM was generated with VirtuoZo™. The resolution of the DSM (grid-based) is 1 meter (Figure 2a), tree stands are observable, and the results seem satisfactory. However, when we checked the initial DSM (using VirtuoZo's interactive DEM Editing Tool module while wearing a stereo-goggle), we found that the errors in the DSM were distributed mainly at the boundaries and their vicinities of the oak stands. This examination (Figure 2b) indicated that tree boundaries, especially those at the down-hill side of tree crowns, were shifted and that the sharp depth discontinuity was smoothed. As explained earlier, such shifting and smoothing phenomena are caused by the improper implementation of the smoothness constraint in the matching process and "blind" interpolation.

Extraction of Shadow Patches and Stand Boundaries in the Original Images

Shadows occur not only near boundaries of tree crowns, but also within crown surfaces and near cliffs. We can use shadow information to correct errors in the DSM. The algorithm will be

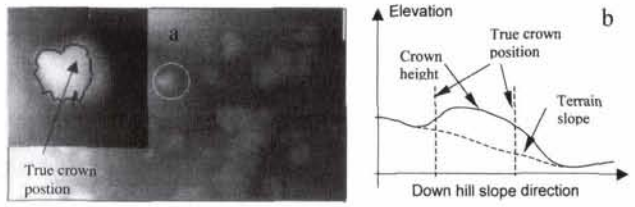

Figure 2. An initial digital surface model (DSM) derived from the stereopair using an existing digital photogrammetric system. (a) The initial DSM. (b) A profile along the down slope direction. The vertical dash-lines are the boundary of the tree and the dash-curve is the ground. The profile shows that the curve is smoothed and includes errors near the boundary of the tree.

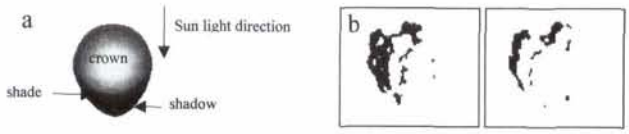

Figure 3. Shadow and shade of a tree canopy. (a) Shadow and its components. (b) The extracted shadow patches.

discussed in the shadow boundary correction section. Shadows can be extracted through image thresholding (Mei, 1996; Shao, 1993). Assuming that shadows are the darkest in the images, image thresholding is suitable for extracting shadows cast by oaktrees and stands. In this paper, we treated a shadow patch as one consisting of shade and shadow (Figure 3a). They were extracted through image thresholding (Figure 3b).

Because tree leaves on oak tree crowns are dense and the canopy surface is relatively smooth, the gray-level values of the oak crowns do not vary a lot from one location to the other on the image (Figure 4). Both oak stands and individual trees can be extracted using image thresholding or classification approaches. The boundary of each oak stand (or tree) can be extracted using a boundary tracking technique. In our study those boundaries were considered as the lines that separate the oak segments from the shadow and background. The boundaries should be closed. Within those individually closed boundaries, the surfaces were considered to be continuously smooth (some approximations are made because the crown surfaces of oak trees in the real world are not strictly continuously smooth). Thus, the errors within the crown interiors were not corrected.

Obtaining 3D Coordinates

The 3D coordinates of those extracted features were calculated based on the image rectification approach. We used ray-tracing (Zhang and Zhang, 1996). The algorithm works following the principle of imaging geometry. Rays are extended from points on canopy boundaries in the original image through the photographic center until the DSM is intersected. Those intersected points are the modeled canopy boundary points. The algorithm tries to find those intersection points on the DSM. Once they are found, their 3D positions become the initial 3D coordinates. The algorithm can then be iterated to refine the 3D coordinates of the crown boundaries.

Correcting Errors on the Stand Boundaries

The two conjugate boundaries, one from the left image and one from the right image of the stereo pair, should be coincident in the 3D world but, because of matching errors, one boundary point may be matched to a non-boundary point in the other image. Therefore, the 3D coordinates of the two conjugate boundaries usually do not coincide with each other (Figure 5a). In order to correct for the discrepancies between the two conjugate boundaries, every point pertinent to the conjugate boundaries is re-matched. The matching is performed in 3D space, not in the image space. In the matching process, the epipolar geometry is used as a constraint to simplify the search for corresponding boundary points. The correct match should be the two points having the minimum distance in the epipolar direction. This matching criterion is chosen because boundaries are very sparse, and it is almost impossible to generate many candidate matches within the search range. The automatically derived DSM provides a good approximation and greatly reduces the search range. In our experiments we found that the discrepancy ranged from 0 to 5 meters, i.e., the maximum search range was ± 5 pixels in the one-meter DSM.

In the 3D matching, most of the boundary points can be matched except a small portion (usually less than 10 percent in our experiments) that has been incorrectly segmented as boundaries. Therefore, those unmatched points are considered as artifacts and are removed from the boundary points. Through the 3D matching step, those portions of wrongly matched boundary points (i.e., with no match in the conventional image matching) are assigned matches. As a result, every point on a boundary gains a match. By back-projecting those matches into the image space, we can obtain their parallax measurements. Based on the parallax measurements and the orientations, the three-dimensional coordinates of those boundaries can be computed. It is at this stage that the coordinates of boundary points are corrected both horizontally and vertically (Figure 5b).

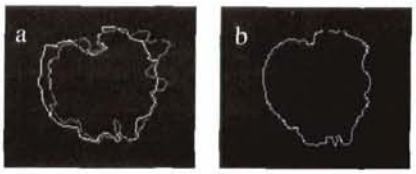

Figure 5. Tree boundary discrepancy correction. (a) White line from the left image and gray line from the right image and they are orthorectified in the 3D coordinate system. The discrepancy shows that matching errors occur at stand boundaries. (b) Results after correction.

Correcting Errors in a Shadow Boundary

A point that casts a shadow and its corresponding shadow point on the ground should lie on a line in the sun light direction (Figure 6). Denote (X_t, Y_t, Z_t) as the 3D coordinates of the point that casts a shadow on the ground with (X_g, Y_g, Z_g) as its 3D shadow coordinates. The sun direction is defined by three cosine elements a, b, and c. The following equations hold:

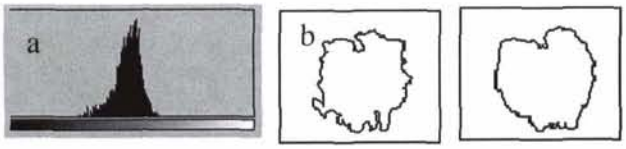

Figure 4. Crown boundaries are extracted through image thresholding. (a) The histogram of the photograph. (b) The extracted stand boundaries based on a threshold determined through histogram analysis.

Figure 6. Examples of shadow geometry violations. The dark points are violations of Equation 1 and the white points are violations of the inequality Equation 3.

$$\frac{(X_t - X_g)}{a} = \frac{(Y_t - Y_g)}{b} = \frac{(Z_t - Z_g)}{c} = constant \qquad (1)$$

where $a \neq 0, b \neq 0, c \neq 0$, (except noon, dawn, and evening). If the time of the day when the photographs were taken is known, the three elements can be determined with the following equations:

$$\begin{cases} a = \cos(Az) \cdot \cos(El + \pi) \\ b = \sin(Az) \cdot \cos(El + \pi) \\ c = \sin(El + \pi) \end{cases} \qquad (2)$$

Note that the unit vector's direction is from the sun to the ground. El is the solar elevation angle and Az is the azimuth angle (Campbell, 1981; Bonhomme, 1993).

Thus,

$$\cos(El) = \sin(\delta) \cdot \sin(\lambda) + \cos(\delta) \cdot \cos(\lambda) \cdot \cos(H)$$

and

$$\cos(Az) = -\cos(\delta) \cdot \sin(H)/\cos(El)$$

where δ is the solar declination, λ is the geographic latitude, and H is the *hour angle*. The solar declination is a function of day of the year: i.e.,

$$\sin(\delta) = 0.39785 \cdot \sin(278.9709 \cdot 0.9856 \cdot J + 1.9163 \cdot \sin(356.6153 + 0.9856 \cdot J))$$

where J is the Julian day.

Boundaries of shadows are divided into two parts: crown points and their cast shadow points, and they should have a one-one correspondence. Using Equation 1, the crown points and their ground counterparts can be identified. Those points missing the one-one correspondence are considered as errors. Through this checking, we can correct for some errors of shadows caused by gray-level thresholding. Shadow points are rematched using image area correlation and new elevation values are assigned to them.

Correcting Errors within the Shadowed Patches

Shadowed points should be below the corresponding sun-light ray, i.e., the following inequality equation holds:

$$Z_g < Z_t \qquad (3)$$

where Z_g is the elevation of the shadow point and Z_t is the elevation of the corresponding point on the crown in the sun-light direction. Those points violating the above relation are discarded and their elevation values are replaced through interpolation.

Correcting Errors in the Occluded Regions

Although occluded regions can be detected using ray-tracing analysis, the computation costs are high because we also need tree height information and slope information for the adjacent ground. However, tree heights are not available at this stage. In order not to fall into an endless loop and to make sure that all the occluded regions are detected, we simply generated a buffer of a certain width around stand boundaries (the corrected boundaries). The buffer zones are initially considered as occluded regions with their width being the widest possible width of occluded regions in the test area.

Tree crown coverage and its surrounding buffers are assigned as "no data." Thus, we gained a new DSM with holes of "no data" (Figure 7). Those "no data" holes are filled with data using data points surrounding those holes. The interpolation is done through polynomial fitting. A new DSM that excludes tree heights is generated.

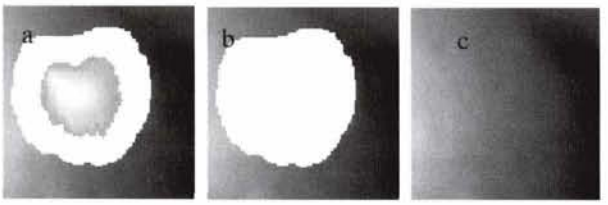

Figure 7. Correction of occluded regions. (a) White donut is the buffer treated as occluded. (b) White region is considered as "no data" and their elevation values assigned through interpolation. (c) The interpolated results.

Correcting Errors Near the Edges on Crowns

Even though some portions of crown near the crown edges are visible both in the left image and in the right image, elevation values at those positions change abruptly, leading to large matching uncertainties. A correction procedure similar to that for occluded regions was applied. Those portions of crowns near the edges are masked out using a distance threshold (Figure 8). Then elevation values are interpolated through inverse distance weighting. Data points used for interpolation are both from the corrected boundary and from the inner parts of the crown. A new DSM can be derived through a logic overlay of the DSM, excluding tree heights and the corrected crown DSM. Elevation values in those places with tree stands in the DSM excluding tree heights are replaced by elevation values of the corrected crown DSM.

Results and Discussions

Ideally, each of the above correction steps should be done simultaneously. However, this is impossible. When we correct for the errors in shadow boundaries, some already corrected crown boundaries may include errors again. Thus, the correction should be made iteratively. Because of image segmentation errors by thresholding, two physically conjugate boundaries may not be correctly extracted from the image. Thus, the techniques used for extraction of shadow patches and oak stand boundaries are critical to correct for the mis-matches.

In order to assess the effect of the correction, stand boundaries and a DSM were interactively collected using VirtuoZo™ digitial photogrammetric software. We compared the results after correction and those before correction using the manually

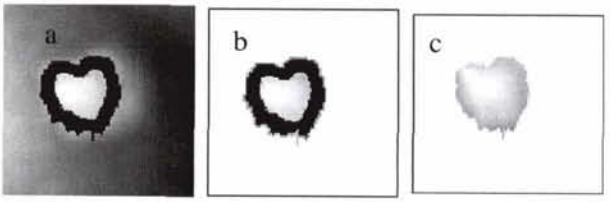

Figure 8. Correction of the crown DSM near the edge. (a) Crown pixels near the boundary marked black. (b) Data in the black region are replaced through interpolation. (c) Results of interpolation.

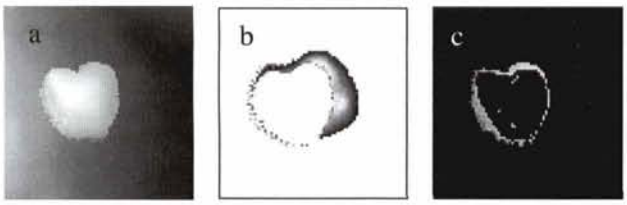

Figure 9. Comparison of the DSMs obtained with different methods. (a) The DSM manually measured through interactive editing as the reference. (b) The difference between the reference DSM and the initial DSM automatically derived before correction. (c) The difference between the reference DSM and the corrected DSM.

collected data as reference (Figure 9a). This can be compared with the DSM directly obtained from digital photogrammetry without postprocessing (Figure 9b), and the DSM after all corrections. Clearly, the postprocessing approach improved the results. We found that 88.3 percent points on the crown boundaries before correction had greater than 1 meter horizontal errors. After error correction greater than 98.6 percent points on the crown boundaries had less than 1 m horizontal errors. Therefore, after the correction the crown boundaries were better located. We also found that 78.4 percent points on crown boundaries before correction had greater than 2 meters elevation errors and after correction greater than 85.6 percent points on crown boundaries were within 2 meters of the reference.

We also observed that the crown closure derived through subtraction of a DSM and a DEM (without forest stands) before correction was 165.4 square meters and after correction it became 133.6 square meters. The reference crown closure was 121.5 square meters. Therefore, through correction, the accuracy of crown closure has been greatly improved. In order to determine the significance of different error sources, we generated three DSMs, each of which has one error source corrected. They were (A) corrected shadow related errors, (B) corrected errors in occluded regions, and (C) corrected errors for the near edge portions of crowns and in the occluded region. The crown closures derived from A, B, and C were 162.7, 117.9, and 136.1 square meters, respectively. From these results, the correction for occluded regions and near crown edges are the most influential in improving crown closure estimation. It seems that our procedure for correcting shadow effects is less effective. Because the effect of shadow is dependent on sun angles, our shadow correction method may work well when shadows are more severe in a photograph. For the photograph used in this study, the shadow patches are sparse and correction is limited only at the boundaries of shadow patches. Nevertheless, shadow related information has been useful in other ways such as for the determination of object heights (Shao, 1993). Accurate tree height will in turn improve occlusion analysis and thus will indirectly contribute to crown closure estimation.

In summary, our approach is essentially a correction method applied to an initial DSM derived from a stereo pair by an existing digital photogrammetry package. It consisted of three steps: (1) boundaries of oak stands and shadows are extracted from the original images; (2) the 3D coordinates of those boundaries are calculated by projecting those boundaries with the DSM, and, (3) violations of the shadow geometry, occlusion, and boundary constraints are detected and corrected in the DSM. The benefit of the corrections lies in the fact that boundaries of oak stands in the initial DSM become more accurately located and the final DSM becomes more accurate. Although this study has been carried out at an oak stand, similar improvements can be expected with other broadleaf forest types. Results of this study indicate that errors caused by violations of the shadow geometry and occlusion constraints can be corrected. The proposed method is feasible and the algorithms are efficient because the new constraints need only be applied to a small portion of the DSM, i.e., at the stand boundaries and their vicinities.

Acknowledgments

This research was partially supported by the University of California Integrated Hardwood Range Management Program, a University of California DANR grant, a USFS grant, and a National Natural Science Foundation of China grant (49825511).

References

Ackerman, F., and P. Krzystek, 1997. Complete automation of digital aerial triangulation, *The Photogrammetric Record*, 15(89):645–656.

Brown, D.G., and A.F., Arbogast, 1999. Digital photogrammetric change analysis as applied to active coastal dunes in Michigan, *Photogrammetric Engineering & Remote Sensing*, 65(4):467–474.

Bonhomme, R., 1993. The solar radiation: Characterization and distribution in the canopy, *Crop Structure and Light Microclimate: Characterization and Applications*, INRA, Paris, France, pp. 17–28.

Campbell, G.S., 1981. Fundamentals of radiation and temperature relations, *Encyclopedia of Plant Physiology*, Vol. 12A , Springer-Verlag, New York, N.Y., pp. 11–40.

Dhond, U.R., and J.K. Aggarwal, 1989. Structure from stereo—A review, *IEEE Transactions on Systems, Man, and Cybernetics*, 19(6):1489–1510.

Fischer, A., T.H. Kolbe, and F. Lang, 1998. Extracting buildings from aerial images using hierarchical aggregation in 2D and 3D, *Computer Vision and Image-Understanding*, 72(2):185–203.

Gong, P., G.S. Biging, S.M. Lee, X. Mei, Y. Sheng, R. Pu, B. Xu, and K-P Schwarz, 1999a. Photo-ecometrics for forest inventory, *Geographic Information Sciences*, 5(1):9–14.

Gong, P., X. Mei, G. Biging, and Z. Zhang, 1999b. Monitoring oak woodland change using digital photogrammetry, *Journal of Remote Sensing, China*. 3(4):285–289 (in Chinese).

Heipke, C., 1996. Overview of image matching techniques, *OEEPE Workshop on the Application of Digital Photogrammetric Workstations*, 09–11 October, Lausanne, Switzerland. See http://dgrwww.epfl.ch/PHOT/publicat/wks96/tocwks96.html.

———, 1997. Automation of interior, relative and absolute orientation, *ISPRS Journal of Photogrammetry and Remote Sensing*, 52(1):1–19.

Hoekman, D.H., and C. Varekamp, 1998. High-resolution single-pass interferometric radar observation of tropical rain forests trees, *Proceedings of the Second International Workshop, Retrieval of Bio- and Geo-Physical Parameters from SAR Data for Land Applications* (M. Borgeaud and T.D. Guyenne, editors), 21–23 October, ESTEC, Noordwijk, The Netherlands (ESA Sp 441, European Space Agency), pp. 233–240.

Ivin, R.B., and D.M. Mckeown, 1989. Methods for exploiting the relationship between buildings and their shadows in aerial imagery, *IEEE Transactions on System, Man and Cybernetics*, 19(6):1564–1675.

Kanade, T., and M. Okutomi, 1994. A stereo matching algorithm with an adaptive window: Theory and experiment, *IEEE Transactions on Pattern Analysis and Machine Intelligence*, 16(9):920–932.

Krzystek, P., and F. Ackerman, 1995. New investigations into the practical performance of automatic DEM generation, *Proceedings, ACSM/ASPRS Annual Convention*, 27 February–02 March, Charlotte, North Carolina, 2:488–500.

Mei, X., Z. Zhang, and J. Zhang, 1996. CSN based extraction of building shadow structures, *Journal of Wuhan Technical University of Surveying and Mapping*, 54(3):265–268 (in Chinese).

Mei, X., P. Gong, and G.S. Biging, 2001, Image matching based on tracking matching paths in the similarity space, *Photogrammetric Engineering & Remote Sensing*, 67(4):453–460.

Mohan, R., and R. Nevatia, 1989. Using perceptual organization to extract 3D structures, *IEEE Transactions on Pattern Analysis and Machine Intelligence*, 11(11):1121–1139.

Shao, J., 1993. *Wavelet Theory and Its Application in Automatic Extraction of Buildings*, Ph.D. thesis, Wuhan Technical University of Surveying and Mapping, Wuhan, China, 125 p. (in Chinese).

Paparoditis, N., M. Cord, and M. Jordan, 1998. Building detection and reconstruction from mid- and high-resolution aerial imagery, *Computer Vision and Image Understanding*, 72(2):122–142.

Sahar, L., and A. Krupnik, 1999. Semiautomatic extraction of building outlines from large-scale aerial images, *Photogrammetric Engineering & Remote Sensing*, 65(4):459–465.

Weidner, U., and W. Förstner, 1995. Towards automatic building extraction from high resolution digital elevation models, *ISPRS Journal of Photogrammetry and Remote Sensing*, 50(4):38–49.

Zhang, Z., and J. Zhang, 1996. *Digital Photogrammetry*, Press of Wuhan Technical University of Surveying and Mapping, Wuhan, China, 214 p. (in Chinese).

(Received 30 June 2000; accepted 31 October 2001)